Water Air Soil Pollut (2011) 217:83–93
DOI 10.1007/s11270-010-0569-8

Monitoring and Modeling Nitrate Persistence in a Shallow Aquifer

Micòl Mastrocicco · Nicolò Colombani · Giuseppe Castaldelli · Nebo Jovanovic

Received: 26 March 2010 / Accepted: 20 July 2010 / Published online: 31 July 2010

Abstract A modeling study on fertilizer by-products fate and transport was performed in an unconfined shallow aquifer equipped with a grid of 13 piezometers. The field site was located in a former agricultural field overlying a river paleochannel near Ferrara (Northern Italy), cultivated with cereals rotation until 2004 and then converted to park. Piezometers were installed in June 2007 and were monitored until June 2009 via pressure transducer data loggers to evaluate the temporal and spatial variation of groundwater heads, while an onsite meteorological station provided data for recharge rate calculations via unsaturated zone modeling. The groundwater composition in June 2007 exhibited elevated nitrate (NO_3^-) and chloride (Cl^-) concentrations due to fertilizer leaching from the top soil. The spatial distribution of NO_3^- and Cl^- was heterogeneous and the concentration decreased during the monitoring period, with NO_3^- attenuation (below 10 mg/l) after 650 days. A transient groundwater flow and contaminant transport model was calibrated versus observed heads and NO_3^- and Cl^- concentrations. Cl^- was used as environmental tracer to quantify groundwater flow velocity and it was simulated as a conservative species. NO_3^- was treated as a reactive species and denitrification was simulated with a first order degradation rate constant. Model calibration gave a low denitrification rate ($2.5e^{-3}$ mg-NO_3^-/l/d) likely because of prevailing oxic conditions and low concentration of dissolved organic carbon. Scenario modeling was implemented with steady state and variable flow time discretization to identify the mechanism of NO_3^- attenuation. It was shown that transient piezometric conditions did not exert a strong control on NO_3^- clean up time, while transient recharge rate did, because it is the main source of unpolluted water in the domain.

Keywords Groundwater modeling · NO_3^- · Cl^- · Unconfined aquifer · Groundwater pollution · Solute transport

M. Mastrocicco · N. Colombani (✉)
Dipartimento di Scienze della Terra, Università di Ferrara,
Ferrara, Italy
e-mail: clo@unife.it

G. Castaldelli
Dipartimento di Biologia ed Evoluzione,
Università di Ferrara,
Ferrara, Italy

N. Jovanovic
CSIR, Natural Resources and Environment,
Stellenbosch, South Africa

1 Introduction

In the last decades, the use of nitrogen fertilizers has increased exponentially at a global scale (Vitousek 1997; Galloway 2008) with detrimental consequences on freshwater and marine ecosystems (Jorgensen and Richardson 1996; Ongley 1996), on nitrous oxide

emissions and greenhouse effect (Turner 1991; Gruber and Galloway 2008). Groundwater (Nolan et al. 2002; Foster 2000) and drinking water contamination (Höring and Chapman 2004) are causing serious health problems worldwide, such as methahemoglobinemia or "Blue Child Syndrome" (Cynthia et al. 2002; Fan and Steinberg 1996), congenital malformations (Dorsch et al. 1984) and different forms of cancer (Hill et al. 1973; Ward et al. 1996).

The European Environment Agency showed that high NO_3^- concentrations in groundwater across the EU (EEA 1999) is a widespread and serious problem. For example in England, over 70% of surface and groundwater NO_3^- originated from agricultural activities (Kraft et al. 2008). A significant fraction of drinking water is exposed to these risks, as supported by the long history of European law amendments for water protection, starting with the Nitrate Directive (OJEC 1991) to the Water Framework Directive (OJEC 2000).

The Po River valley is the largest Italian alluvial plain and is heavily affected by agricultural pollution, especially NO_3^- (Onorati et al. 2006; Cinnirella et al. 2005; Giuliano 1995). In addition to synthetic nitrogen fertilizers, intense livestock farming and a high population density produce an unsustainable nitrogen load. Mass balance calculations have indicated that, in some districts, theoretical nitrogen load from all cited sources accounts for more than 1,000 kg N ha^{-1} $year^{-1}$ (Palmeri et al. 2005) which is a much larger amount than any maximum crop nitrogen uptake.

Once manure or synthetic urea are distributed, several physical and biological processes regulate the fate of hydrolyzed ammonia. Ammonia may adsorb onto soil particles, be assimilated by crops, volatilized to the atmosphere, or be nitrified to nitrate. Nitrate may be assimilated by crops as well or lost in runoff water and, more likely, be leached to the water table and be partly denitrified along the way to N_2O or to N_2, with an irreversible loss of nitrogen to the atmosphere (Shomar et al. 2008; Bernot and Dodds 2005; Burt et al. 1999; Martin et al. 1999). In fact, when water percolates in the subsurface, oxygen (O_2) may quickly decline and NO_3^- can be employed by denitrifying bacteria as electron acceptor (Appelo and Postma 2005). In certain soils, the degree of water saturation is the most important variable, regulating oxygen mobility and consequently, oxidative conditions at microscales, where denitrification takes place (Fenchel et al. 1998). Organic matter availability is the other regulator of denitrification (Hofstra and Bouwman 2005) and if labile substrates are not abundant, denitrification occurs at small rates and NO_3^- can travel long distances within aquifers (Bölke and Denver 1995).

Following this rationale, a small-scale field site within a shallow unconfined aquifer was monitored to quantify the time required to completely remove NO_3^-. In 2004, the field site was converted into a recreational area and no more N fertilizers were applied on it and upstream of it. Thus, this experiment represents an example of integral NO_3^- protection area of particular interest since the field site lies on a river paleochannel, a preferential geological structure for contaminants migration (Spalding et al. 1993; Meinardus et al. 2002). The main focus of this study was to determine the mechanism of NO_3^- attenuation or persistence in groundwater. For this purpose, the data set was used to implement scenario modeling to evaluate the role of recharge and aquifer flow transient conditions in NO_3^- natural attenuation.

2 Materials and Methods

2.1 Field Site

The study site, consisting of a monitoring grid of 40× 40 m, is located in a rural area (44°51′32 N, 11°39′15 E) between the town of Ferrara and the Po River main course, at about 100 km from the outlets into the Adriatic Sea, NE Italy (Fig. 1). The test site has been investigated with a combination of core logs and electrical resistivity tomography (ERT) techniques, from which a conceptual and numerical flow model was established (Mastrocicco et al. 2009). Briefly, the hydrogeological units present in the test site are the unconfined aquifer composed of recent fluvial sandy deposits with clay and silt lenses (from 0 to around 5 m b.g.l.) and the underlying aquiclude constituted of clay and silt sediments (from 5 to almost 14 m b.g.l.). The site was cultivated from 1986 to 2004 under a rotation of cereals, mainly maize and wheat, using urea as nitrogen fertilizer at an average rate of 300 kg/ha/year. From September 2004, the field was converted into a park with grass cover. Since then, no fertilizers and other agrochemicals were applied. Potential nitrate

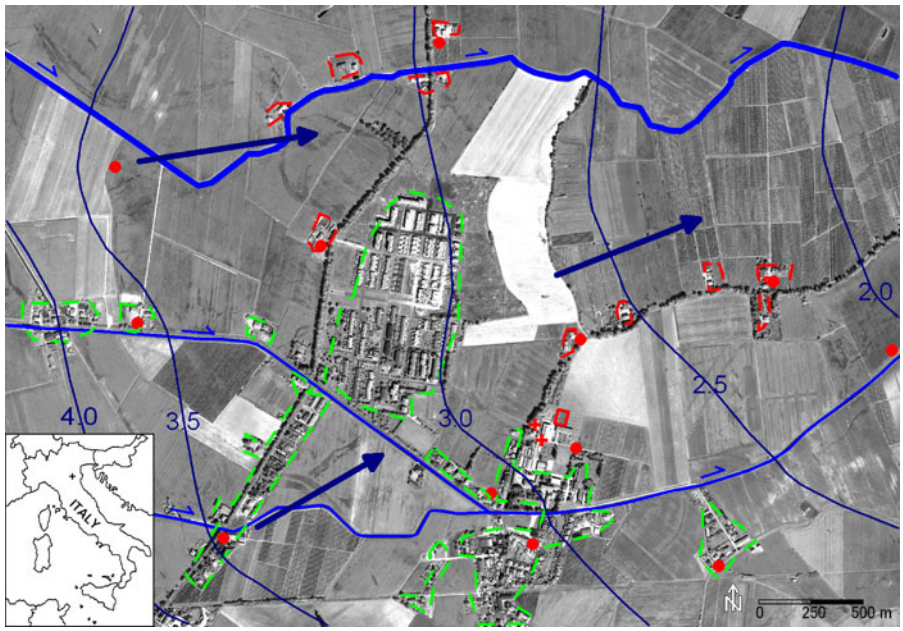

Fig. 1 Location of the study area and potential nitrate point sources, i.e., isolated houses not connected to the sewage network (*red rectangle*) and recent buildings connected to the sewage network (*green dashed areas*); principal canals (*light blue lines*) and their direction (*light blue arrows*); contour lines of groundwater elevation in m above sea level (*dark blue lines*), principal groundwater directions (*dark blue arrows*) and location of shallow groundwater wells (*red dots*) used for groundwater elevation monitoring and for chemical analysis (*red crosses*)

sources from upstream were not detected from existing shallow boreholes located immediate upstream of the field site (see Fig. 1), which never showed nitrate ammonium and nitrite concentrations above 3 mg/l. At the end of May 2007, piezometers were installed to monitor groundwater flow in the unconfined aquifer of the paleochannel. Piezometric variations during the year were attributed to variable recharge rate and water level changes in canals surrounding the study area. Evapotranspiration played an important role in determining recharge rate but it was not directly controlling the heads fluctuation since maximum root depth of grass was 0.3 m b.g.l., while groundwater table usually lied 2 m b.g.l and it was unlikely that the root system was fed by capillary rise.

2.2 Analytical and Field Methods

LTC M10 Levelogger Solinst® dataloggers were placed in piezometers A3, C1, C5, and E3 (Fig. 2) to monitor hourly groundwater level, electrical conductivity, and temperature. The other piezometers were monitored for groundwater level and sampled after low-flow purging for major ions determination during eight surveys. Vertical aquifer discretization was accomplished by straddle removable packers sampling, each piezometer was sampled every meter via low flow purging and sampling method.

A meteorological station recording daily rainfall, wind speed, temperature, and humidity was located on the field site while solar radiation data were recorded in another station located 4.6 km from the

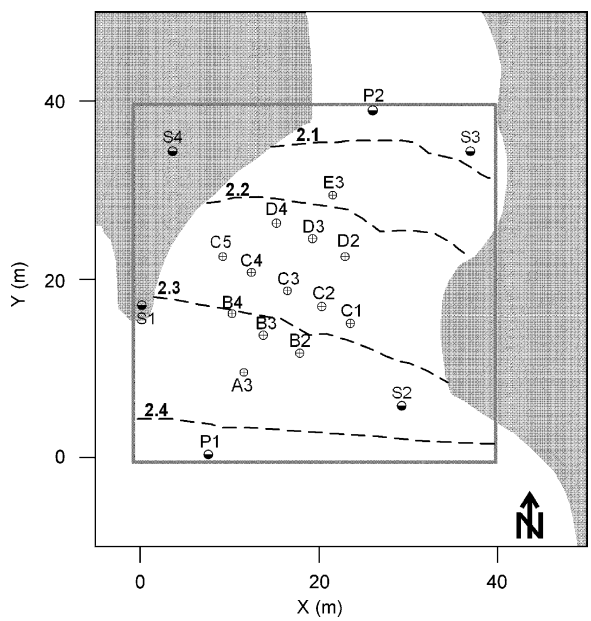

Fig. 2 Plan view of the site, in *gray* are the paleochannel boundaries, *cross-circles* are the monitoring wells, *half circles* P1 and P2 are the piezometers used for heads boundaries and S1, S2, S3, S4 are the core logging sites used to characterize the unsaturated zone

site. Data are available on-line from the meteorological regional service (www.dexter.it).

The unsaturated zone was sampled at the beginning of this study by means of auger coring. Four samples were taken at depths from 0 to 2 m b.g.l. (Fig. 2), and sediments were analyzed for major anions and cations. Unsaturated zone sediment analysis consisted of a batch with a sediment/water ratio of 1:10, using 10 g of air dried sample dispersed in 100 ml of Milly-Q water (Millipore, USA). A biological inhibitor (1 g/l phenylmercuric acetate) was added to prevent microbial activity and the solution was stirred for 1 h and then allowed to stand for 1 day. The insoluble residue was removed by filtration and analyzed for major cations and anions.

In-well parameters were determined with the HANNA Multi 340i instrument which includes a HIcell-31 pH combined electrode with a built-in temperature sensor for pH measurements, a CellOx 325 galvanic oxygen sensor for DO measurements, a combined AgCl-Pt electrode for Eh measurement and a HIcell-21 electrode conductivity cell for EC measurements. Samples were filtered through 0.22 μm Dionex vial caps. The major cations, anions and oxianions (acetate and formate) were determined with isocratic dual pump ion chromatography ICS-1000 Dionex, equipped with an AS9-HC 4×250 mm high capacity column and an ASRS-ULTRA 4 mm self-suppressor for anions, and a CS12A 4×250 mm high capacity column and a CSRS-ULTRA 4 mm self-suppressor for cations. An AS-40 Dionex auto-sampler was employed to run the analyses, quality control (QC) samples were run every ten samples. The standard deviation for all QC samples run was better than 4%. Charge balance errors in all analyses were less than 5% and predominantly less than 3%. Organic carbon was determined with a carbon analyzer (Carbon Analyzer Shimadzu TOC-V-CSM) after acidification with one drop of 2 M HCl to remove dissolved carbonate.

2.3 Modeling

Recharge was assumed to occur homogeneously over the study area; the recharge rate was calculated with the finite element model HYDRUS-1D (Šimunek et al. 2008). The HYDRUS-1D numerical grid was subdivided in 200 nodes of 0.01 m each, to form a regular 2 m long grid. The grid was subdivided into two regions representing the upper (from top soil to 0.8 m b.g.l.) and the lower soil horizons (0.8–2 m b.g.l.). Initial water content conditions of collected soil cores (every 0.25 m) at each site were measured with the gravimetric method and interpolated linearly along the vertical axis.

At the soil surface, variable flux and head conditions were selected to represent the atmospheric boundary. Daily reference evapotranspiration was calculated with the FAO-56 recommended Penman–Monteith equation (Allen et al. 1998). It was assumed that the grass cover at the experimental site resembles the reference surface as defined by Allen et al. (1998). Potential transpiration and evaporation were split using an estimated surface cover fraction of 0.8 (Ritchie 1972). Root water uptake was simulated using the grass dimensionless water stress response function available in the HYDRUS-1D database (Feddes et al. 1978). Run-off was assumed negligible due to the flat topography and based on other studies in this area (Antonellini et al. 2008). Soil hydraulic parameters were assigned using default values included in the soil catalog of HYDRUS-1D for silt-loam (upper layer) and sand (lower layer). Free drainage was selected as lower boundary condition and the cumulative bottom flux allowed the estimation of groundwater recharge for different periods.

A fully transient 3D flow model using MODFLOW-2005 was implemented and calibrated versus heads monitored in 13 observation wells recorded during eight piezometric campaigns, and versus continuous data recorded with the A3, C1, C5, and E3 piezometers. The piezometric campaigns were performed on the following dates: 19/06/07, 18/07/07, 18/08/07, 29/09/07, 17/01/08, 4/08/08, 10/02/09, and 16/06/09. The numerical grid of MODFLOW-2005 was discretized by a regularly spaced grid of 0.5×0.5 m. Vertically, between 4.3 and −1.7 m a.s.l., the model domain was discretized into six layers each of 1 m thickness to represent vertical variations in hydraulic conductivity. The permeability distribution was derived by a combination of multi level slug tests and ERT techniques (Mastrocicco et al. 2009). The total simulation time of 730 days (from 18 June 2007 to 17 June 2009) was subdivided into 13 different stress periods to reproduce groundwater fluctuations recorded with dataloggers. The number of stress periods was selected after preliminary modeling using an initial number of 110 stress periods, then decreas-

ing the number of stress periods until the correlation coefficient (R^2) of the heads residuals (difference between calculated and measured values) started decreasing compared to the initial value. This exercise allowed obtaining the minimum number of stress periods needed to achieve an accurate simulation of the heads temporal variation. The time-variant specified-head package (Harbaugh et al. 2000) was used to represent the northern and southern boundaries. No flow was assumed along the eastern and western sides, since they consist of impermeable silty clay sediments (Mastrocicco et al. 2009). Recharge rate was assigned by summing up the daily recharge calculated with HYDRUS-1D in each stress period, and it was assumed uniform across the model domain.

The transport and reaction processes were simulated using MT3DMS code (Zheng and Wang 1999). Transport parameters like longitudinal, transversal, and vertical dispersivity were initially assumed to be 2, 0.2, and 0.02 m, the molecular diffusion coefficient was assumed to be $1e^{-9}$ m^2/s (Gelhar 1993), while the effective porosity was assumed to be 0.3 for sandy sediments and 0.4 for silty sediments. The advection dispersion term was solved using the total variation diminishing scheme with a Courant number of 0.1, since it is the most robust numerical solution method and is virtually free of numerical dispersion. Dispersivity and effective porosity parameters were adjusted via trial and error calibration (Zheng and Bennett 2002) to fit the Cl^- concentrations observed in eight sampling campaigns performed at the same time as the piezometric campaigns. After calibration of the conservative transport model fitted well Cl^- observed concentrations (where only dilution processes were accounted for), the denitrification rate was determined by tuning it at incremental steps (via trial and error calibration) to fit the NO_3^- observed concentrations.

3 Results and Discussion

3.1 Unsaturated Zone Characterization and Recharge Estimation

Low concentrations of mineral nitrogen species were found in the unsaturated zone (from 0 to 2 m b.g.l.) from auger coring at the beginning of the experiment. Average NO_3^- and Cl^- concentrations were respectively 2.5±0.4 and 4.7±2.6 mg/kg of dried sediments, while nitrite and ammonium were found occasionally, always at concentrations close to the limit of detection (0.10 ppm for nitrite and 0.30 ppm for ammonium). The very low concentration of mineral nitrogen found in the soil resulted from leaching after the cessation of fertilizer use in April 2004. At the beginning of this study, the highest groundwater concentrations of NO_3^- and Cl^- (used as conservative tracer) were 102.0 and 201.1 mg/l, respectively, while average concentration were 34.2 and 87.6 mg/l. Very low concentrations of organic carbon were present in groundwater, with an average value of 0.83 mg/l and a standard deviation of 0.56 mg/l. This suggests a carbon limiting condition for denitrification (Rivett et al. 2008).

From Fig. 3, it is evident that actual evapotranspiration (ET_a) takes place throughout the year, although at slower rates during winter time because the evaporative demand is less pronounced. The precipitation distribution pattern is bimodal with maximum peaks in autumn and spring, and sparse storm events during summer periods. This is typical of sub-coastal temperate climates characterized by cold winters and warm summers (Pavan et al. 2008). The cumulative rainfall in the monitoring period was 1,586 mm, while estimated recharge was 599 mm. The 2007/08 season was much drier than 2008/2009, and the calculated recharge was 147 mm in 2007/08 and 452 mm in 2008/09. From Fig. 3, it is also evident that recharge took place only during late winter–early spring.

3.2 Transient Groundwater Flow Model

The transient flow model was calibrated without changing the parameters of the original model (Mastrocicco et al. 2009); only boundary conditions were updated for the additional monitoring period with actual measured heads. The absolute residual mean (ARM) error was 0.058 m with a normalized root mean square (NRMS) error of 5.79% and a R^2 of 0.97. Figure 4 shows the overall good match between observed and calculated heads and the time series highlight a cyclical variation of the piezometric heads with minimum values at the end of the summer season and peaks during spring. The groundwater fluctuation was mainly driven by the canal located upgradient as shown in Fig. 4, while recharge during the late winter and spring seasons prevented the ground-

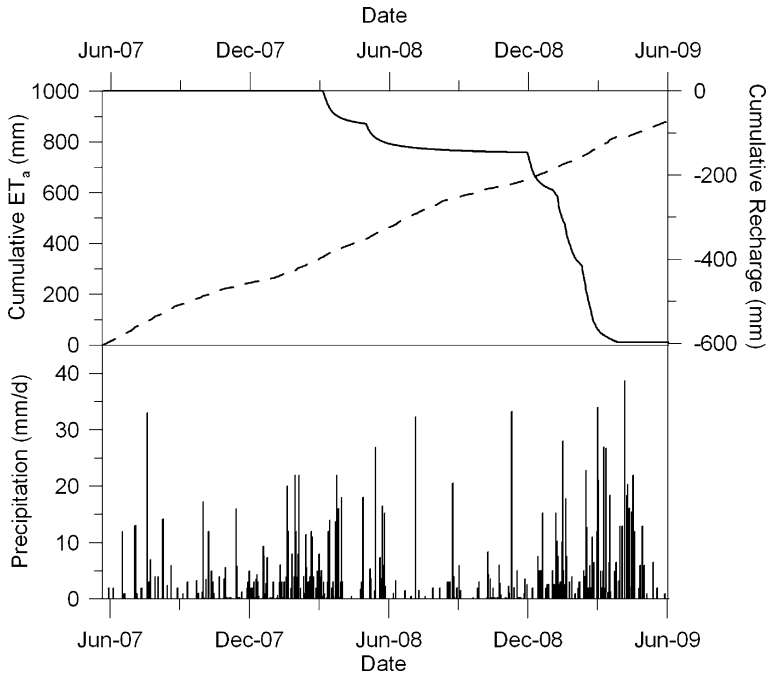

Fig. 3 Calculated cumulative actual ET_a plotted with a *dashed line*, calculated cumulative recharge (*upper plot*) plotted with a continuous line, and daily rainfall (*lower plot*) recorded with the onsite meteorological station

water to suddenly drawdown when the canal level decreased.

The groundwater flow was always in the direction from A3 to E3, since the piezometric level of the latter was always lower than the former; but the hydraulic gradient varied during the year, as the head difference between A3 and E3 was not constant. Variable flow therefore occurred during the year. In the high recharge period (during winter 2008/09), the head difference became very small and a flat groundwater table established.

3.3 Transient Solute Transport Model

The initial concentrations of Cl^- and NO_3^-, observed in the first survey on 19/06/07, displayed a similar

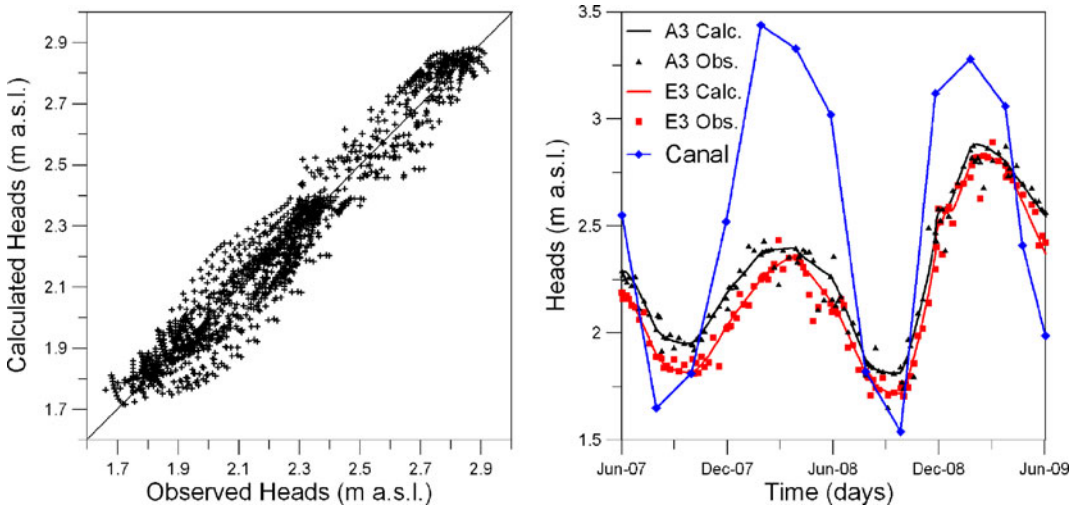

Fig. 4 Scatter diagram of the calibrated transient flow model comparing observed and computed heads in all observation wells (*left*) and time series graph comparing observed and computed heads of two piezometers at the opposite sides of the monitoring grid, A3 and E3 (*right*)

spatial distribution pattern (Fig. 5). This pattern was captured by multi-level sampling, with increasing concentrations from the model inflow (lower side) to the model outflow (upper side).

The concentration distribution, with increasing values from the inflow to the outflow, was due to gradual replacement of NO_3^- polluted groundwater with NO_3^- free (≈1 mg/l) groundwater coming from upstream and through recharge.

Trial and error calibration of dispersivity and porosity produced satisfactory results with little variation from the initial values; in fact, only longitudinal dispersivity was adjusted, while its ratio with transversal and vertical dispersivity was left unchanged. Final values were 0.53, 0.053, and 0.0053 m for longitudinal, transversal, and vertical dispersivity, respectively. These low values suggest a relatively homogeneous transport of solutes dominated by advection. Effective porosity also needed a small refinement of initial values with final values of 0.31 for sandy sediments and 0.42 for silty sediments. The calibrated conservative transport model showed a good match between calculated and observed concentrations (Fig. 6), with an ARM error of 5.43 mg/l, a NRMS error of 4.54%, and a R^2 of 0.977.

A decrease in Cl^- concentration was recorded from the beginning of the monitoring period in all observation wells, approaching the pristine Cl^- concentration (from 28 to 41 mg/l) at the end of the monitoring period. The initial difference in Cl^- concentration in the wells shown in Fig. 6 was due to dilution processes with pristine groundwater and through recharge. Probably, a cyclical Cl^- input through agricultural amendments (that was stopped in 2004) provided elevated Cl^- in the whole area, but since monitoring started in 2007, the dilution effect was more evident in the wells located upstream with respect to those located downstream. A complete clean up from Cl^- was reached within the monitoring grid at the end of summer 2008, although it is difficult to provide an exact time when Cl^- concentrations became stable.

The behavior of NO_3^- was similar to Cl^-, since a decrease in concentration was recorded from the

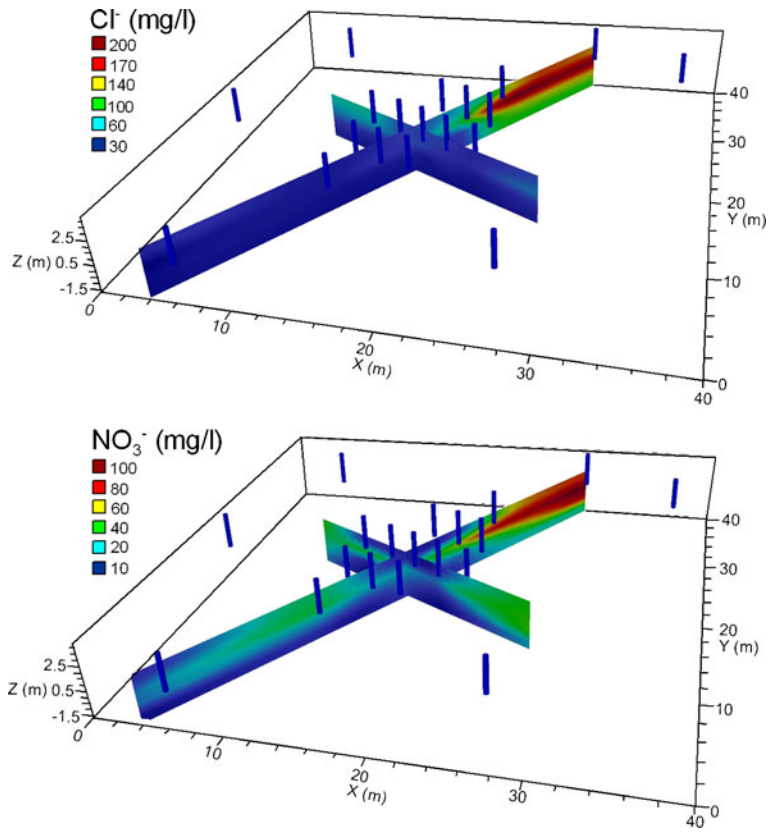

Fig. 5 Three-dimensional box plot contour maps of initial observed Cl^- and NO_3^- concentrations and location of monitoring wells

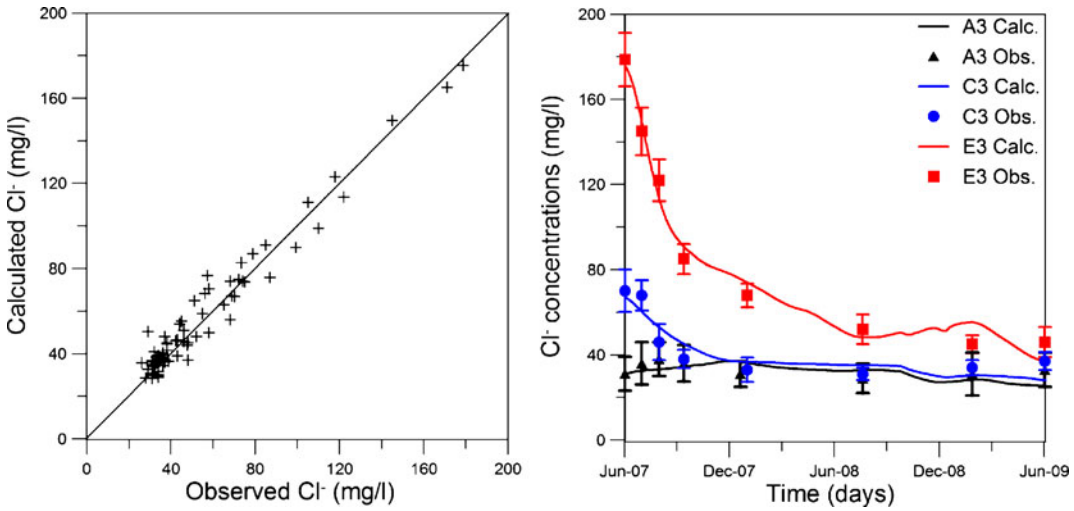

Fig. 6 Scatter diagram comparing observed and computed Cl^- concentrations in all observation wells (*left*) and time series graph comparing observed and computed Cl^- concentrations in piezometers A3, C3 and E3 (*right*)

beginning of the monitoring period. NO_3^- reached concentrations below 10 mg/l in January 2009 (Fig. 7). Simulated NO_3^- concentrations fitted reasonably well observed data using a first order degradation rate of $2.5e^{-3}$ mg-NO_3^-/l/d, but the scatter plot of Fig. 7 shows a less accurate fit compared to Cl^-.

However, an ARM error of 4.11 mg/l, a NRMS error of 5.71%, and an R^2 of 0.960, indicated that the reproduction of observed concentrations was still robust. In addition, the calibrated numerical model was compared to a conservative (no degradation) NO_3^- dilution scenario and to a higher degradation rate ($5e^{-3}$ mg-NO_3^-/l/d) scenario. The NO_3^- conservative scenario showed that (at least after the first year of monitoring) the observed concentrations cannot be matched with calculated ones, as observed NO_3^- were always lower than those calculated (Fig. 7). A 100% increase of the degradation rate produced unrealistically low NO_3^- concentrations. Consequently, model results were found to be sensitive to changes in the degradation rate input value. To quantify this aspect

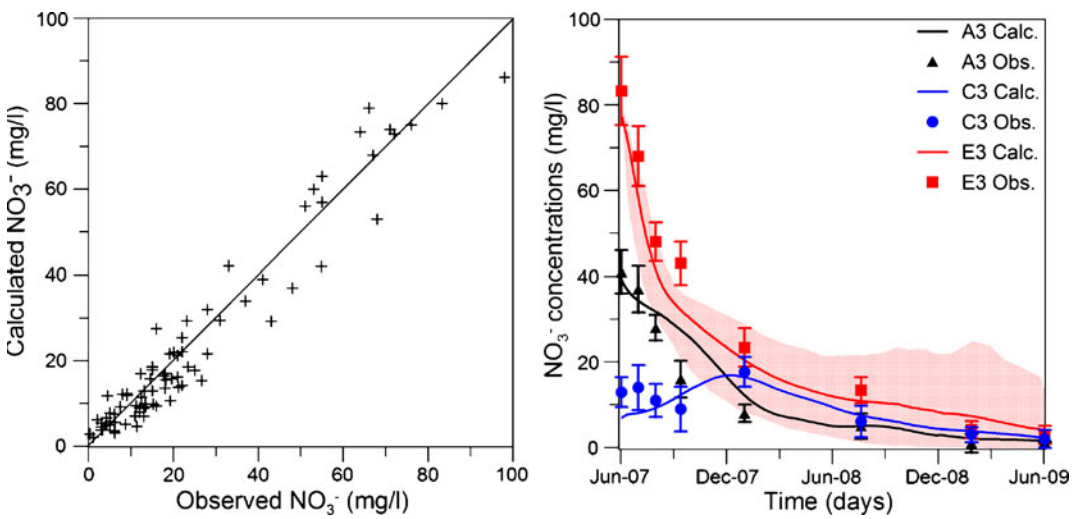

Fig. 7 Scatter diagram comparing observed and computed NO_3^- concentrations in all observation wells (*left*) and time series graph comparing observed and computed NO_3^- concentrations in piezometers A3, C3 and E3 (*right*). The shaded area shows results for E3 without degradation (*upper area border*) and with a doubled degradation rate (*lower area border*)

Table 1 Scenario modeling with decreasing number of stress periods (Sp.) from the fully transient calibrated model to a simple steady state model.

Scenarios	Recharge	Head Boundaries
Transient calibrated model 1	13 Sp.	13 Sp.
Transient scenario 2	4 Sp.	13 Sp.
Transient scenario 3	1 Sp.	13 Sp.
Transient scenario 4	13 Sp.	5 Sp.
Transient scenario 5	4 Sp.	5 Sp.
Transient scenario 6	1 Sp.	5 Sp.
Transient scenario 7	13 Sp.	1 Sp.
Transient scenario 8	4 Sp.	1 Sp.
Steady state 9	1 Sp.	1 Sp.

the normalized sensitivity coefficient (Zheng and Bennett 2002) was calculated for a 100% perturbation of the NO_3^- degradation rate with respect to the total computed mass of NO_3^- during the simulation, and found to be 0.26.

3.4 Comparison with Steady State Results

The results obtained from transient flow and transport models were judged satisfactory. Despite this, numerical models often assume steady state flow conditions and this may not be representative of field conditions. To clarify this aspect, a series of numerical scenarios were run. The transient flow model boundary conditions were time variant heads and variable recharge rate; both these terms were varied by means of scenario modeling. In general, the first term contributes significantly to change the average flow velocity field, while the second term contributes to dilution processes through recharge. Different scenarios were built up and compared to the transient calibrated model (Table 1). Starting from the most complex transient model, the temporal discretization was decreased toward steady state conditions, by decreasing the number of stress periods, Sp (Table 1). Flow model results in each scenario were compared to piezometric heads measured only at corresponding stress periods. Consequently, the steady state scenario was compared against average piezometric heads.

Results of the flow simulations are summarized in Fig. 8. A deterioration of R^2 is appreciable when a decreasing number of stress periods are employed. The steady state scenario displayed poorer statistics in comparison with the calibrated model (AMR from 0.058 m to 0.045 m, NRMS from 5.79% to 8.49%); this is due to the averaging of all observed and calculated heads. The small value of AMR error in the steady state simulation is not due to a close fit between observed and calculated heads, but it occurred because the average heads used to calibrate the steady state model had a variation range of just a few centimeters within the piezometers grid, while the transient model was calibrated versus transient head data which span over 1.2 m (see Fig. 4), and consequently the head residuals were higher in the transient model. The comparison between the calibrated transient model and the other scenarios was performed also for the conservative and reactive transport simulations (Fig. 8). In this case, a deterioration of simulation results is appreciable only for the conservative tracer simulation. This was probably due to a major dilution effect most evident for the initial elevated Cl^- concentrations (not shown), while this effect was smoothed out for NO_3^-. The same effect was present in all scenarios because the flow field was changed and subsequently the conservative transport of Cl^- was principally affected by this change. A closer inspection of Fig. 8 reveal that variable recharge is affecting the reactive and non-reactive transport more than the flow field variations. In fact, the NO_3^- and Cl^-

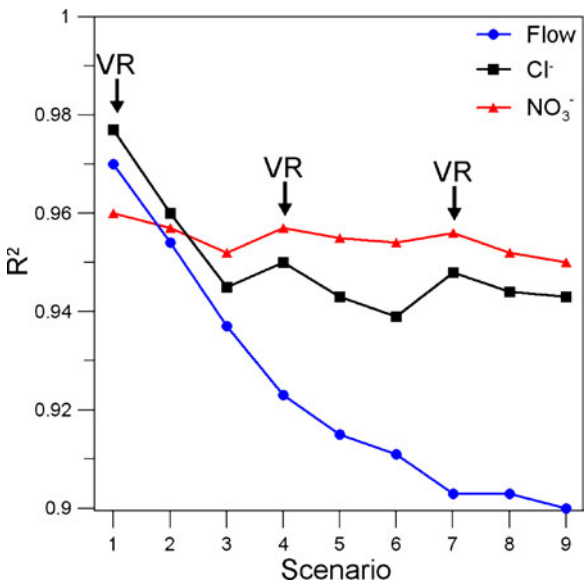

Fig. 8 Plot of R^2 for flow simulation, conservative transport (Cl^-) and reactive transport (NO_3^-) of each scenario described in Table 1, the scenarios with variable recharge rate are indicated with an arrow and the acronym "VR"

best-fit scenarios were obtained using a variable recharge (transient scenario 1, 4, and 7).

4 Conclusions

A small field-site experiment was established to evaluate the clean-up time of a shallow unconfined aquifer contaminated by NO_3^-. The site represents a case of vulnerable area (river paleochannel) where agricultural practices were stopped. NO_3^- persistence in the field confirmed the high vulnerability of unconfined aquifers to this common pollutant and the long bioremediation time required. NO_3^- removal within the monitoring grid appeared to be mainly driven by dilution processes. The three-dimensional flow and transport modeling provided a useful tool to asses NO_3^- fate, discriminating the higher effect of dilution compared to the lower effect of degradation by denitrification. The value of degradation rate determined in this study is comparable to those found recently for unconfined aquifers under agricultural fields (Green et al. 2008). Scenario modeling provided evidence that in a flat area, like the one of this study, recharge is one of the key parameters in NO_3^- remediation. The flow field may not significantly affect NO_3^- clean up time due to the small head gradients in these areas (usually 1‰), which are not sufficient to induce large seasonal heads and flow variations. Thus, an accurate estimation of recharge rate should be taken into account when evaluating clean up times especially in intensively cultivated areas, where a yearly input of nitrogen from fertilizer may not easily allow a noticeable effect on NO_3^- removal.

Acknowledgments The work presented in this paper was made possible and financially supported by the L.A.R.A.-ENVIREN project, under PRITT fund, PARCAGRI (Delib. CIPE n°202) and by the Provincial Administration of Ferrara, within the UE-Water Project of the South-East Europe Program. A special thank to the Fondazione F.lli Navarra which hosted the site and gave detailed information on agricultural practices and to ARPA SIMC for the meteorological data. Dr. Enzo Salemi and Dr. Umberto Tessari are acknowledged for their technical support.

References

Allen, R. G., Pereira, L. S., Raes, D., & Smith, M. (1998). Crop evapotranspiration. Guidelines for computing crop water requirements. Irrigation and Drainage Paper No. 56. FAO, Rome.

Antonellini, M., Mollema, P., Giambastiani, B., Bishop, K., Caruso, L., Minchio, A. et al. (2008). Saltwater intrusion in the coastal aquifer of the southern Po plain Italy. *Hydrogeology Journal*, *16*(8), 1541–1556. On-line version: http://dx.doi.org/10.1007/s10040-008-0319-9

Appelo, C. A. J., & Postma, D. (2005). *Geochemistry, groundwater and pollution* (2nd ed.). Rotterdam: Balkema.

Bernot, M. J., & Dodds, W. K. (2005). Nitrogen retention, removal, and saturation in lotic ecosystems. *Ecosystems, 8*, 442–453.

Bölke, J. K., & Denver, J. M. (1995). Combined use of groundwater dating, chemical, and isotopic analyses to resolve the history and fate of NO3- contamination in two agricultural watersheds, Atlantic coastal plain, Maryland. *Water Resources Research, 31*(9), 2319–2339.

Burt, T. P., Matchett, L. S., Goulding, K. W. T., Webster, C. P., & Haycock, N. E. (1999). Denitrification in riparian buffer zones: the role of floodplain hydrology. *Hydrological Processes, 13*(10), 1451–1463.

Cinnirella, S., Buttafuoco, G., & Pirronea, N. (2005). Stochastic analysis to assess the spatial distribution of groundwater NO3- concentrations in the Po catchment (Italy). *Environmental Pollution, 133*, 569–580.

Cynthia, A., Voelker, M., Lee Brown, M., Roger, M., & Hinson, M. (2002). Preoperatively acquired methemoglobinemia in a preterm infant—Case report. *Pediatric Anesthesia, 12*, 284–286.

Dorsch, M. M., Scragg, R. K. R., McMichael, A. J., Baghurst, P. A., & Dyer, K. F. (1984). Congenital malformations and maternal drinking water supply in rural South Australia—A case-control study. *American Journal of Epidemiology, 119*, 474–486.

EEA, European Environmental Agency. (1999). Groundwater quality and quantity in Europe, 123 pp. (http://www.eea.europa.eu/publications/groundwater07012000)

Fan, A. M., & Steinberg, V. E. (1996). Health implications of nitrate and nitrite in drink water: An update on methemoglobinemia occurrence and reproductive and developmental toxicity. *Regulatory Toxicology and Pharmacology, 23*, 35–43.

Feddes, R. A., Kowalik, P. J., & Zaradny, H. (1978). *Simulation of field water use and crop yield*. Wageningen: Pudoc.

Fenchel, T., King, G. M, & Blackburn, T. H. (1998). Bacterial Biogeochemistry: the ecophysiology of mineral cycling. Second Edition, Academic Press, ISBN 0-12-103455-0.

Foster, S. S. D. (2000). Assessing and controlling the impacts of agriculture on groundwater—From barley barons to beef bans. *Quarterly Journal of Engineering Geology and Hydrogeology, 33*(4), 263–280.

Galloway, J. N. (2008). Transformation of the nitrogen cycle: recent trends, questions, and potential solutions. *Science, 320*, 889–892.

Gelhar, L. W. (1993). *Stochastic subsurface hydrology* (p. 390). Old Tappan: Prentice-Hall.

Giuliano, G. (1995). Ground water in the Po basin: some problems relating to its use and protection. *The Science of the Total Environment, 171*, 17–27.

Green, C. T., Puckett, L. J., Böhlke, J. K., Bekins, B. A., Phillips, S. P., Kauff man, L. J., et al. (2008). Limited occurrence of denitrification in four shallow aquifers in agricultural areas of the United States. *Journal of Environmental Quality, 37*, 994–1009.

Gruber, N., & Galloway, J. N. (2008). An Earth-system perspective of the global nitrogen cycle. *Nature, 451*, 293–296.

Harbaugh, A. W., Banta, E. R., Hill, M. C., & Mc Donald, M. G. (2000). MODFLOW-2000, The U.S. G. S. modular ground-water model, User guide to modularization concepts and the ground-water flow process, U. S. G. S. Open-file report 00-92.

Hill, M. J., Hawksworth, G., & Tattersall, G. (1973). Bacteria, nitrosamines and cancer of the stomach. *British Journal of Cancer, 28*, 562–567.

Hofstra, N., & Bouwman, A. F. (2005). Denitrification in agricultural soils: summarizing published data and estimating global annual rates. *Nutrient Cycling in Agroecosystems, 72*, 267–278.

Höring, H., & Chapman, D. (2004). NO3-s and nitrites in drinking water. In: World Health Organization Drinking Water Series. London: IWA Publishing

Jorgensen, B. B., & Richardson, K. (1996). *Eutrophication in coastal marine ecosystems. Coastal and estuarine studies, 52* (p. 273). Washington DC: American Geophysical Union.

Kraft, G. J., Browne, B. A., DeVita, W. M., & Mechenich, D. J. (2008). Agricultural pollutant penetration and steady state in thick aquifers. *Ground Water, 46*(1), 41–50.

Martin, T. L., Kaushik, N. K., Trevors, J. T., & Whiteley, H. R. (1999). Review: denitrification in temperate climate riparian zones. *Water, Air, and Soil Pollution, 111*, 171–186.

Mastrocicco, M., Vignoli, G., Colombani, N., & Abu Zeid, N. (2009). Surface electrical resistivity tomography and hydrogeological characterization to constrain groundwater flow modeling in an agricultural field site near Ferrara (Italy). *Environmental Earth Sciences Journal*. doi:10.1007/s12665-009-0344-6.

Meinardus, H. W., Dwarakanath, V., Ewing, J., Hirasaki, G. J., Jackson, R. E., Jin, M., et al. (2002). Performance assessment of NAPL remediation in heterogeneous alluvium. *Journal of Contaminant Hydrology, 54*, 173–193.

Nolan, B. T., Hitt, K. J., & Ruddy, B. C. (2002). Probability of NO3- contamination of recently recharged groundwaters in the conterminous United States. *Environmental Science & Technology, 36*(10), 2138–2145.

Official Journal of the European Communities (1991). Directive 91/676/EEC of the European Parliament and Council Directive of the 12 December 1991 concerning the protection of waters against pollution caused by NO3-s from agricultural sources, 8p.

Official Journal of the European Communities (2000). Directive 2000/60/EC of the European Parliament and Council Directive of the 23 October 2000 establishing a framework for Community action in the field of water policy, 72p.

Ongley, E. D. (1996). Control of water pollution from agriculture: FAO irrigation and drainage. Paper 55: Rome.

Onorati, G., Di Meo, T., Bussettini, M., Fabiani, C., Farrace, M. G., Fava, A., et al. (2006). Groundwater quality monitoring in Italy for the implementation of the EU water framework directive. *Physics and Chemistry of the Earth, 31*, 1004–1014.

Palmeri, L., Bendoricchio, G., & Artioli, Y. (2005). Modelling nutrient emissions from river systems and loads to the coastal zone: Po River case study, Italy. *Ecological Modelling, 184*, 37–53.

Pavan, V., Tomozeiu, R., Cacciamani, C., & Di Lorenzo, M. (2008). Daily precipitation observations over Emilia–Romagna: Mean values and extremes. *International Journal of Climatology, 28*(15), 2065–2079.

Ritchie, J. T. (1972). Model for predicting evaporation from a row crop with incomplete cover. *Water Resources Research, 8*(5), 1204–1213.

Rivett, M. O., Buss, S. R., Morgan, P., Smith, J. W. N., & Bemment, C. D. (2008). Nitrate attenuation in groundwater: A review of biogeochemical controlling processes. *Water Research, 42*, 421–4232.

Šimunek, J., Šejna, M., Saito, H., Sakai, M., & van Genuchten, M Th. (2008). *The HYDRUS-1D Software Package for Simulating the Movement of Water, Heat, and Multiple Solutes in Variably Saturated Media, Version 4.0, HYDRUS Software Series 3, Department of Environmental Sciences* (p. 315). Riverside: University of California, Riverside.

Shomar, B., Osenbrück, K., & Yahya, A. (2008). Elevated NO3- levels in the groundwater of the Gaza Strip: Distribution and sources. *The Science of the Total Environment, 398*, 164–174.

Spalding, R. F., Exner, M. E., Martin, G. E., & Snow, D. D. (1993). Effects of sludge disposal on groundwater nitrate concentrations. *Journal of Hydrology, 142*(1–4), 213–228.

Turner, R. E. (1991). Fertilizer and climate change. *Nature, 349*, 469–470.

Vitousek, P. M. (1997). Human alteration of the global nitrogen cycle: Sources and consequences. *Ecological Applications, 7*, 737–750.

Ward, M. H., Mark, S. D., Cantor, K. P., Weisenburger, D. D., Correa-Villasenor, A., & Zahm, S. H. (1996). Drinking water nitrate and the risk of non-Hodgkin's lymphoma. *Epidemiology, 7*(5), 465–471.

Zheng, C., & Bennett, G. D. (2002). *Applied contaminant transport modeling* (2nd ed.). New York: Wiley. 621.

Zheng, C., Wang, P. P. (1999). MT3DMS: A modular three-dimensional multispecies model for simulation of advection, dispersion and chemical reactions of contaminants in groundwater systems; Documentation and User's Guide, Contract Report SERDP-99-1; US Army Engineer Research and Development Center: Vicksburg, MS.